Solution and Solid-State Characterization of Highly Rigid, Eight-Coordinate Lanthanide(III) Complexes of a Macrocyclic Tetrabenzylphosphinate†

Silvio Aime,*,‡ Andrei S. Batsanov,§,∥ Mauro Botta,‡ Judith A. K. Howard,§ David Parker,*,§ Kanthi Senanayake,§ and Gareth Williams§

Dipartimento di Chimica Inorganica, Chimica Fisica dei Materiali dell'Universita degli Studi di Torino, V.P. Giuria 7, 10125 Torino, Italy, and Department of Chemistry, University of Durham, South Road, Durham DH1 3LE, U.K.

Received December 10, 1993⊗

The ligand 1,4,7,10-tetraazacyclododecanetetrakis(methylenebenzylphosphinic acid), **1**, forms kinetically stable complexes with lanthanide ions (Ln = Eu, Gd, Tb, Yb, and Y) which are eight-coordinate (no bound water), with single diastereoisomers being preferentially formed (*RRRR* or *SSSS* at each stereogenic phosphorus centre). The ^{1}H NMR spectra for the Eu and Yb complexes have been assigned and no significant fluxional behavior is observed in the temperature range 5-80 °C at 400 MHz. The gadolinium complex is a promising outer-sphere contrast agent for magnetic resonance imaging, and analyses of variable temperature NMRD profiles suggest that the nearest water molecule is 4.25 Å distant from Gd (cf. 3.82 Å for the *P*-Me analogue). A relatively strong complex is formed with bovine serum albumin ($K_d = 2.8 \times 10^{-4}$ dm^3 mol^{-1}) leading to a significantly enhanced relaxivity in which a major contribution may arise from the exchange of mobile protons on the protein which undergo rapid dipolar relaxation caused by the proximity of the paramagnetic Gd ion. The crystal structures of the monohydrochloride salt of the free ligand and of the anionic yttrium(III) complex (as its oxonium salt) are reported. In the structure of the yttrium complex there is no metal-bound water molecule, with the nearest water being 5.62 Å from the yttrium atom. Crystal data for [(**1**)H]Cl: monoclinic, *C2/c*, $a = 48.21(3)$ Å, $b = 11.455(4)$ Å, $c = 18.474(11)$ Å, $\beta = 103.88(4)°$, $V = 9905(9)$ Å^3, $Z = 8$, 2484 reflections, $R = 0.078$. Crystal data for H_3O[Y(**1**)]: orthorhombic, *Pbcn*, $a = 22.332(5)$ Å, $b = 23.052(9)$ Å, $c = 21.301(8)$ Å, $V = 10\,965$ Å^3, $Z = 8$, 1625 reflections, $R = 0.089$.

Introduction

Lanthanide(III) complexes with octadentate macrocyclic ligands have been the object of several studies recently in view of their use as contrast agents (CA) in magnetic resonance imaging (MRI)[1] and their potential as luminescent probes in analytical and clinical chemistry.[2] The high kinetic stability of the complexes (with respect to dissociation) is an essential requirement for their in vivo use.[3,4] Among the large number of octadentate ligands reported in the literature, only in complexes with TETA is the lanthanide ion presented with a coordination number of 8, i.e. no water molecules in its inner coordination sphere.[5a] In fact in the context of relaxometric studies of aqueous solutions of Gd(III) complexes, [GdTETA]$^-$ is considered a model system[5b] for evaluating the contribution of the water protons. Here, we consider a new class of octacoordinated lanthanide(III) complexes with octadentate ligands based on the structure of the tetraazacyclododecane ring. The synthesis of the phosphinate ligands $12N_4P_4R_4$ (R = Bz, Me), **1** and **2**, has already been reported[3,6] as well as the

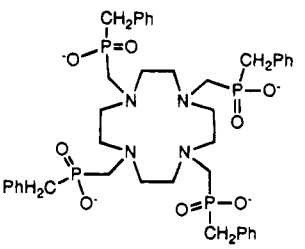

1

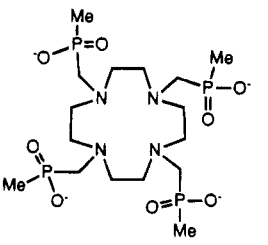

2

preparation of their Y(III) and Gd(III) complexes. These complexes possess attractive properties in terms of *in vivo* stability, excretion pathway, and, in the Gd(III) complex case, considerable potential utility as a CA.[7] We have studied by NMR techniques the solution structure of the complexes by exploiting the close similarity of the chemical behavior and the structural features among the lanthanide(III) ions and the large variations in their magnetic properties. The diamagnetic Y(III) complex allows the application of the routine high resolution multinuclear NMR techniques for structural determination. The paramagnetic complexes with ions such as Eu(III), Dy(III), and

† Abbreviations: TETA is 1,4,8,11-tetraazacyclotetradecanetetraacetic acid; DOTA is 1,4,7,10-tetraazacyclododecanetetraacetic acid;[1] DOTP is 1,4,7,10-tetraazacyclododecanetetrakis(methylenephosphonic acid).

‡ Universita degli Studi di Torino.

§ University of Durham.

∥ On leave from the Institute of Organoelement Compounds, Russian Academy of Science, Moscow, Russia.

⊗ Abstract published in *Advance ACS Abstracts,* September 1, 1994.

(1) (a) Lauffer, R. B. *Chem. Rev.* **1987,** *87,* 901. (b) Koenig, S. H.; Brown, R. D. *Prog. NMR Spectrosc.* **1990,** *22,* 487.

(2) Soini, E.; Hemmila, I.; Dhalen, P. *Ann. Biol. Clin.* **1990,** *48,* 567. Evangalista, R. A.; Pollak, A.; Allore, B.; Templeton, E. F.; Morton, R. C.; Diamandis, E. P. *Clin. Biochem.* **1988,** *21,* 173.

(3) Parker, D.; Pulukkody, K.; Norman, T. J.; Royle, L.; Harrison, A. *J. Chem. Soc., Perkin Trans. 2* **1993,** 605.

(4) Parker, D.; Jankowski, K. J. In *Advances in Metals in Medicine*; Abrams, M. J., Murrer, B. A., Eds.; Jai Press: New York, 1993; Vol. 1, Chapter 2, pp 29-73.

(5) (a) Spirlet, M. R.; Rebizant, J.; Loncin, M. F.; Desreux, J. F. *Inorg. Chem.* **1984,** *23,* 4278. (b) Xhang, X.; Chang, C. A.; Brittain, H. G.; Garrison, J. M.; Telser, J.; Tweedle, M. F. *Inorg. Chem.* **1992,** *31,* 5597.

(6) Cole, E.; Broan, C. J.; Jankowski, K. J.; Pulukkody, K.; Parker, D.; Millican, A. T.; Beeley, N. R. A.; Millar, K.; Boyce, B. A. *Synthesis* **1992,** 67.

(7) Harrison, A.; Royle, L.; Walker, C.; Pereira, C.; Parker, D.; Pulukkody, K.; Norman, T. J. *Magn. Reson. Imaging* **1993,** *11,* 761.

0020-1669/94/1333-4696$04.50/0

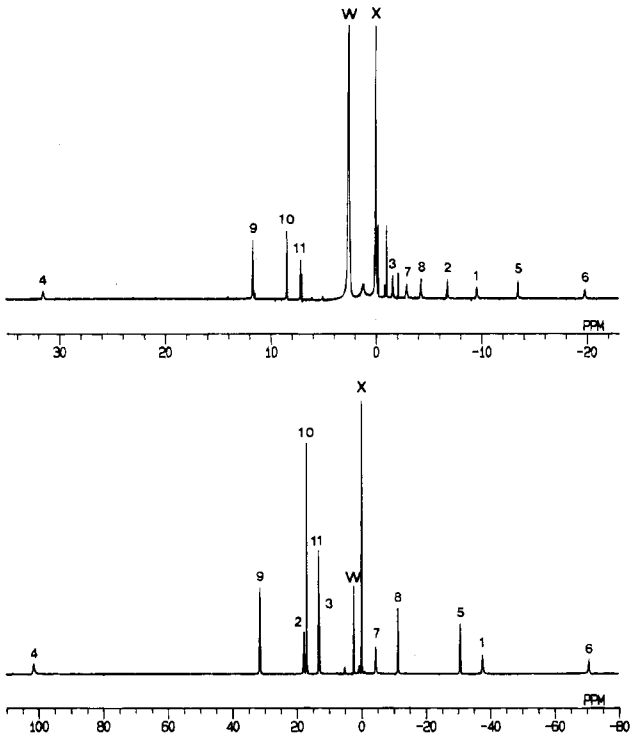

Figure 1. 400 MHz ^{1}H NMR spectra (D_2O, 298 K) of (a) $[Eu(1)]^-$ (top) and $[Yb(1)]^-$ (bottom). The resonances have been labeled according to Scheme 1. The "W" and "X" labels refer to the HOD and ^{t}BuOH signals respectively. ^{t}BuOH was added as an internal reference.

Yb(III), characterized by short values of the electronic relaxation time ($\tau_S \sim 10^{-13}$ s), allow the measurements of high resolution NMR spectra in which the isotropically shifted resonances, spanning an expanded spectral region, contain a large amount of information. The Gd(III) ion with its long value of τ_S produces a dramatic broadening of the NMR signals and thus precludes the recording of high resolution spectra but, alternatively, is able to catalyze the nuclear relaxation of the water protons with a rate constant which depends on the magnetic field and on several structural and dynamic parameters of the complex. Furthermore an X-ray determination has been accomplished for the Y(III) complex of **1** and for the monoprotonated free ligand which reveals the aquation state of the complex.

Results and Discussion

NMR Studies. The ^{1}H NMR spectra of $[Y(1)]^-$ has already been reported[3] and shows, in addition to the aromatic resonances, eight multiplets corresponding to the H_1-H_8 protons. In Figure 1, the 400-MHz ^{1}H NMR spectra of $[Eu(1)]^-$ and $[Yb(1)]^-$ are shown to consist of eleven singlets. The rather different NMR spectral pattern for $[Eu(1)]^-$ and $[Yb(1)]^-$ arises essentially from the occurrence of a large contact contribution to the paramagnetic shift in the proton spectrum of the europium complex. In the case of the Eu(III) complex the transverse relaxation times, T_2, of the proton resonances are sufficiently long to allow the detection of cross-peaks in the 2D homonuclear COSY experiment. Indeed, at lower magnetic field strength (corresponding to a proton Larmor frequency of 90 MHz) it is possible to detect the coupling pattern of several resonances. On the basis of these experiments and by comparison with published data on structurally related complexes,[8] it is possible to assign the 11 resonances according to the labeling of Chart 1.

(8) Aime, S.; Botta, M.; Ermondi, G. *Inorg. Chem.* **1992**, *31*, 4291.

Chart 1

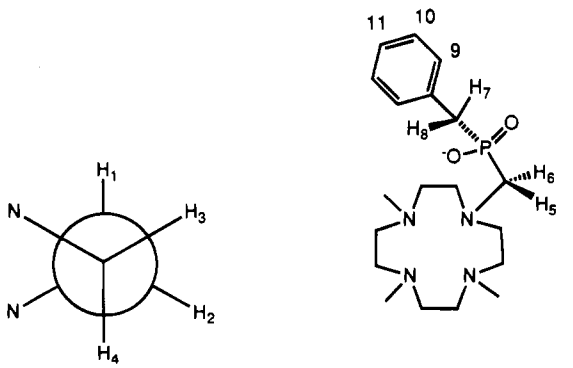

The proton spectrum of the Yb(III) complex covers a much larger chemical shift range and is characterized by a severe paramagnetically-induced line broadening that prevents the recording of a 2D-COSY experiment. Very helpful for the elucidation of the solution structure of $[Yb(1)]^-$ is the comparison with the corresponding $[YbDOTA]^-$ complex, which has been shown to be present in solution as a mixture of two isomers.[8] It is well established that among the lanthanide(III) ions Yb(III) causes paramagnetic shifts essentially free of any contact contribution.[11] Thus the proton chemical shifts can be directly correlated to the structural features of the complex. It is evident that the ^{1}H NMR chemical shifts of the ring and $N-CH_2-P$ protons for $[Yb(1)]^-$ are very strictly related to those for the minor isomer of the corresponding DOTA complex, and therefore it may be concluded that the two compounds in solution have the same inverted square-antiprismatic structure. Interestingly, this structural coordination geometry, largely less important in the DOTA complexes,[9,10] is the only one detectable for the tetrakis(benzylphosphinate) ligand system, thus confirming the suggestion that, on passing from an acetate to a more sterically demanding substituted phosphinate group, this arrangement becomes thermodynamically favored.

The ^{1}H NMR spectra of the three complexes (Y, Eu, Yb) are essentially unchanged in the temperature range 5−80 °C, indicative of a high rigidity of the coordination cage. This stereochemical rigidity is particularly remarkable in respect to the dynamic process involving both the macrocyclic ring and the coordinating arms that occur with the related DOTA and DOTP complexes. On the basis of these findings the relaxation properties of the Gd(III) complexes of **1** and **2** were examined in detail.

Luminescence Measurements. The emission spectrum of $[Eu.1]^-$, (H_2O, 298 K), recorded following excitation at 250 nm, has been assigned, (Figure 2), in terms of the various $^5D_0 \rightarrow {}^7F_n$ transitions. (Quantum yields and lifetimes for $[Eu(1)]^-$ and $[Tb(1)]^-$ and the corresponding complexs with **2** have been reported previously:[25] $[Eu(1)]^-$ in H_2O ($\tau = 1.59$ ms, $\phi = 1 \times 10^{-3}$) and in D_2O ($\tau = 2.07$ ms, $\phi = 1.5 \times 10^{-3}$); $[Tb(1)]^-$ in H_2O ($\tau = 4.13$ ms, $\phi = 0.44$) and in D_2O (4.44 ms, $\phi = 0.49$). Hence the hydration state[32] of the *excited* state of the complex is 0.15 for Eu(**1**) and 0.07 for Tb(**1**). The hydration state is 0.27 for both $[Eu(2)]^-$ and $[Tb(2)]^-$). In nonaxial ligand fields (i.e. those without a C_3 axis or higher), three components are expected for the $^5D_0 \rightarrow {}^7F_1$ transition in europium(III) complexes while only two components may be observed in axially symmetric complexes.[26,27] Indeed, this difference has been

(9) EuDOTA: Spirlet, M.; Rebizant, J.; Desreux, J. F. *Inorg. Chem.* **1984**, *23*, 359. GdDOTA: Dubost, J.-P.; Leger, M.; Langlois, M.-H.; Meyer, D.; Schaefer, M. *C. R. Acad. Sci. Paris Ser. 2* **1991**, *312*, 349.

(10) YDOTA: Parker, D.; Pulukkody, K.; Batsanov, A.; Smith, F. C.; Howard, J. A. K. *J. Chem. Soc., Dalton Trans.* **1994**, 689.

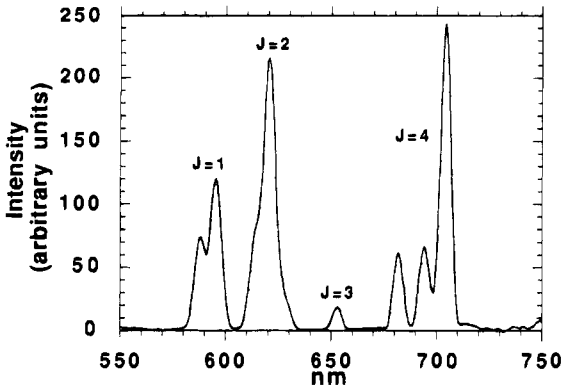

Figure 2. Corrected emission spectrum of $[Eu(\mathbf{1})]^-$ (pH 5.5, H_2O, 293 K) with an excitation wavelength of 250 nm, showing $^5D_0 \rightarrow {}^7F_n$ transitions.

proposed as a simple method of determining the symmetry of lanthanide shift reagents in solution.[28] The appearance of two bands in the $^5D_0 \rightarrow {}^7F_1$ region in $[Eu(\mathbf{1})]^-$ (Figure 2) is consistent with a 4-fold symmetry axis for the complex. The absence of a $^5D_0 \rightarrow {}^7F_0$ transition (at 579 nm[29]) in $[Eu(\mathbf{1})]^-$ is also consistent with the axial symmetry of the complex. This transition is only formally allowed in complexes of low-symmetry.[30] The $^5D_0 \rightarrow {}^7F_1$ transition is magnetic-dipole allowed and so its intensity is relatively unaffected by the Eu(III) coordination environment. The $^5D_0 \rightarrow {}^7F_2$ transition is electric-dipole allowed and is absent or very weak in complexes where the europium lies on an inversion center.[30] Furthermore the transition is hypersensitive: a dramatic dependence of the emission intensity on ligand polarizability is usually observed.[31] Thus the high intensity of the $^5D_0 \rightarrow {}^7F_2$ transition in $[Eu(\mathbf{1})]^-$ is consistent both with the absence of an inversion centre and with the relatively polarizable nature of the Eu(III) environment. A further feature of interest is the high intensity of the $^5D_0 \rightarrow {}^7F_4$ transition relative to the $^5D_0 \rightarrow {}^7F_1$; such a phenomenon has also been observed in the emission spectra of the structurally related EuDOTA and EuTETA complexes.[26]

NMRD Measurements. In order to be considered as a potential contrast agent (CA) for MRI, a paramagnetic complex must satisfy several requirements such as low toxicity, relatively rapid excretion after administration, good water solubility, low osmolality of the solutions clinically used, and high efficiency in catalyzing the water proton relaxation rate.[1] This latter property is commonly described as *relaxivity*, i.e. the increment of the water proton relaxation rate per unit concentration of the paramagnetic CA. It strictly depends, for a given metal ion, upon the structural, electronic and dynamic properties of the complex. Usually, among the lanthanides, attention is primarily focused on complexes of Gd(III) since this metal ion with a high S state electronic structure ($S = {}^7/_2$) couples a large magnetic moment with a long electron spin relaxation time ($\sim 10^{-9}$ s), two properties that ensure an optimum efficiency for nuclear spin relaxation.[11] In general, water proton relaxation rates are altered by the presence of a CA in solution through two distinct mechanisms: inner- and outer-sphere. The inner sphere contribution to the relaxivity (R_p^{is}) arises from the dipolar interaction between the paramagnetic metal ion and the proton nuclei of the directly coordinated water molecules ($q \geq 1$), modulated by the molecular reorientation (τ_R), electron spin relaxation (τ_S), and chemical exchange (τ_M). This latter phenomenon is sufficiently fast, for Gd(III) complexes (1−10 ns), to provide the means of transferring the interaction to the bulk water.

The outer sphere mechanism, which represents the only contribution to relaxivity (R_{1p}^{os}) for complexes with $q = 0$, involves the electron−nuclear magnetic dipolar coupling which occurs when the solvent molecules approach the metal complex during their translational diffusion motion. In this case, the interaction is modulated by the relative translational diffusion of solute and solvent D and by the electronic relaxation time τ_S. The net paramagnetic contribution to the measured water proton relaxation rate (R_{1p}) in a solution containing the metal complex is then given by the sum of these two terms:

$$R_{1p}^{\text{means}} = R_{1p}^{\text{is}} + R_{1p}^{\text{os}} \tag{1}$$

The inner-sphere contribution, as described by the Solomon−Bloembergen−Morgan theory, is given by the following set of equations:[11b,12]

$$R_{1p}^{\text{is}} = \frac{Cq}{55.6}\left(\frac{1}{T_{1M} + \tau_M}\right) \tag{2}$$

$$T_{1M} = \frac{K}{r^6} f(\tau_C, \omega_I, \omega_S) \tag{3}$$

Here C is the molar concentration of the paramagnetic complex, q is the number of water molecules coordinated to the metal ion, T_{1M} is the longitudinal proton relaxation time, and τ_M is the mean residence lifetime in the coordination sites. The relaxation time of the bound water molecules (eq 3) depends on the inverse of the sixth power of the distance r between the metal ion and the water protons, on the Larmor frequencies for the proton (ω_I) and electron (ω_S) and on the correlation time τ_C for the modulation of the dipolar interaction, which is dependent, through an inverse relation, on τ_R, τ_M, and τ_S (eq 4).

$$1/\tau_c = 1/\tau_R + 1/\tau_S + 1/\tau_M \tag{4}$$

The outer sphere term R_{1p}^{os} may represent a sizable contribution to the observed relaxation rate for low molecular weight Gd^{3+} complexes,[13] and it is normally described through Freed's equation, originally suggested for the study of the interaction between stable free radicals and organic solvent molecules:[14]

$$R_{1p}^{\text{os}} = (32\pi/405)\gamma_H^2 g^2 \mu_B^2 S(S+1)(N_A/1000)(C/aD) \times f(\tau_s, \tau_D, \omega_I, \omega_S) \tag{5}$$

Here N_A is Avogadro's number, a is the distance of closest approach between the paramagnetic center and the water molecules, and $\tau_D = a^2/D$. Furthermore it is important to note that the longitudinal water proton relaxation rate is magnetic field dependent not only directly through eqs 3 and 5 but also because the parameter τ_S, which enters the same equations, is itself field-dependent as given by the Morgan equation

$$\tau_s^{-1} = \frac{1}{5\tau_{SO}}\left[\frac{1}{1 + \omega_S^2 \tau_v^2} + \frac{4}{1 + 4\omega_S^2 \tau_v^2}\right] \tag{6}$$

where τ_{SO} is the value of the electronic relaxation time at zero-

(11) (a) Jesson, J. P. In *NMR of paramagnetic Molecules*; La Mar, G. N., Horrocks, W. DeW., Eds.; Academic Press Inc.: New York, 1973; pp 1−51. (b) Bertini, I.; Luchinat, C. *NMR of Paramagnetic Molecules in Biological Systems*; Benjamin, Cummings: Boston, MA, 1986.

(12) Solomon, I. Relaxation Processes in a System of Two Spins. *Phys. Rev.* **1955**, *99*, 559. Bloembergen, N.; Morgan, L. O. *J. Chem. Phys.* **1961**, *34*, 842.

(13) Aime, S.; Botta, M.; Ermondi, E. *J. Magn. Reson.* **1991**, *92*, 572.

(14) Freed, J. H. *J. Chem. Phys.* **1978**, *68*, 4034.

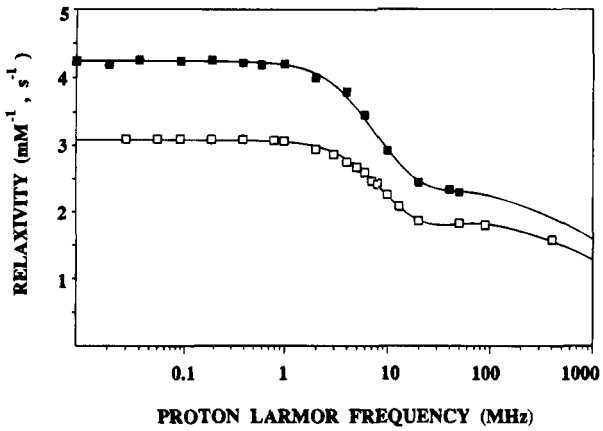

Figure 3. Experimental NMRD profiles (pH 7.3) for [Gd(**1**)]$^-$ (□, 298K) and [Gd(**2**)]$^-$ (■, 296K). The solid lines through the data have been calculated with the parameters of Table 1.

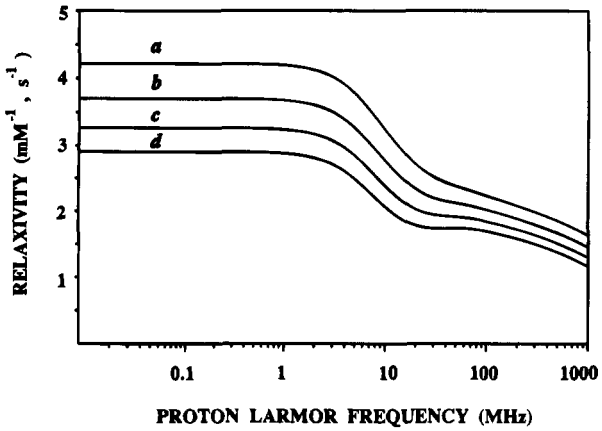

Figure 4. Simulated outer sphere NMRD profiles for values of the distance a of 3.6 (a), 3.9 (b), 4.2 (c), and 4.5 Å (d). Values typical of Gd(III) complexes were utilized for the other parameters: τ_{SO} = 80 ps; τ_V = 15 ps; $D = 2.0 \times 10^{-5}$ cm^2 s^{-1}.

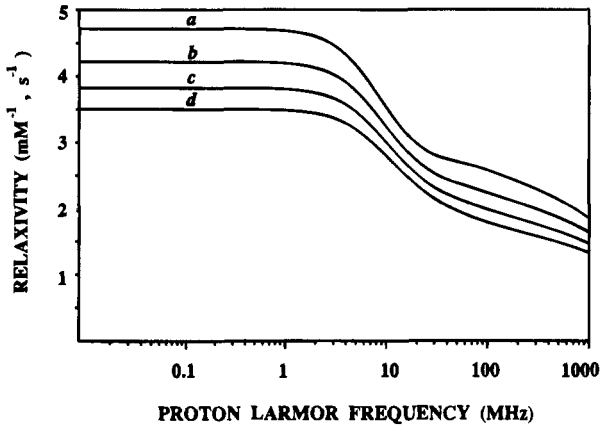

Figure 5. Simulated outer sphere NMRD profiles for values of the diffusion coefficient D of 1.7×10^{-5} (a), 2.0×10^{-5} (b), 2.3×10^{-5} (c), and 2.6×10^{-5} cm^2 s^{-1} (d). Values typical of Gd(III) complexes were utilized for the other parameters: τ_{SO} = 80 ps; τ_V = 15 ps; a = 3.6 Å.

field and τ_v is the correlation time characterizing the time-dependence of the interaction responsible for the relaxation process.

It is apparent that the large structural and dynamic information content of solvent relaxation rate determination when Gd(III) complexes are present in solution can be conveniently exploited only through a magnetic field dependent study. Experimentally this can be done with the field-cycling relaxometer developed by Koenig and Brown,[15] which allows the automatic measurement of the longitudinal water proton relaxation rate in a magnetic field range corresponding to proton Larmor frequencies of 0.01−50 MHz. What is obtained is the so-called nuclear magnetic relaxation dispersion (NMRD) profile, which can be analyzed with the above equations. A large number of profiles have been reported over the last few years for Gd(III) complexes of DOTA- and DTPA-like ligands which have shown some regular and general trends. The relaxivity in the high magnetic field region (~10−50 MHz) is mainly controlled by the value of τ_R, directly proportional to the molecular size, and has about a 50% contribution from the outer sphere mechanism. At low magnetic fields the relaxivity receives a sizable contribution from τ_S, whose value has been shown to depend upon the symmetry around the metal ion and the chemical nature of the coordinating group.[16,17] The exchange lifetime normally neither contributes to τ_C nor influences the NMRD profile since it has an estimated value of the order of the nanoseconds and is then much shorter than T_{1M} (eq 2, fast exchange condition). On the basis of the similar axially symmetric structures of LnP_4R_4 complexes compared with one of the isomers of the LnDOTA chelates, similar NMRD profiles for their corresponding Gd(III) complexes are expected. The experimental NMRD profile for [Gd(**1**)]$^-$ and [Gd(**2**)]$^-$ recorded at 25 and 23 °C, respectively, and at pH = 7.3 are shown in Figure 3. The magnitude of the relaxivity over the entire magnetic field range and the shape of the profiles indicate that both complexes do not have any water molecule directly coordinated and relax the solvent only through outer sphere effects. This is very unexpected on the basis of the close structural similarity of these complexes with several other carboxylate and[16−18] phosphonate[19] complexes derived from the same tetraazacyclododecane ring, where the Gd(III) ion possesses a coordination number of 9. Thus [Gd(**1**)]$^-$ and [Gd(**2**)]$^-$ represent the first examples of macrocyclic complexes based on the 12-N_4 ring where Gd(III) has a coordination number of 8. Furthermore, we note in Figure 3 how different the NMRD profiles are over the entire magnetic field range investigated for two structurally very similar complexes and thus how sensitive this technique is to the chemical environment of the metal ion. The inflection point in the profile correspond to the condition $\omega_S\tau_D \sim 1$, and thus the different inflection points for the two complexes implies a different τ_D value for [Gd(**1**)]$^-$ and [Gd(**2**)]$^-$. Now, since both complexes have both a similar coordination cage and an equal net charge but different molecular size, we may anticipate that they must differ in the value for the parameter a, the distance of closest approach of diffusing water protons to the paramagnetic center.

In Figures 4−6 are reported the simulated NMRD profiles for an "outer sphere" complex where the parameters a, D, and τ_{SO} respectively have been varied around some typical values for Gd(III) chelates in order to better appreciate the effects of each parameter on the profiles. It is clear that by increasing a from 3.6 to 4.5 Å (Figure 4) the inflection point shifts to lower fields and the relaxivity decreases in the entire magnetic field

(15) Koenig, S. H.; Brown, R. D., III. *Relaxometry of Tissue in NMR Spectroscopy of Cells and Organisms*; Gupta, R. M., Ed., CRC Press: Boca Raton, FL, 1987; Vol. II, 75−114.
(16) Sherry, A. D.; Brown, R. D.; Geraldes, C. F. G. C.; Koenig, S. H.; Kuan, K.-T.; Spiller, M. *Inorg. Chem.* **1989**, *28*, 620.
(17) Aime, S.; Botta, M.; Ermondi, G.; Fedeli, F.; Uggeri, F. *Inorg. Chem.* **1992**, *31*, 1100.
(18) Aime, S.; Anelli, P. L.; Botta, M.; Fedeli, F.; Grandi, M.; Paoli, P.; Uggeri, F. *Inorg. Chem.* **1992**, *31*, 2422.
(19) Aime, S.; Botta, S.; Terreno, E.; Anelli, P. L.; Uggeri, F. *Magn. Reson. Med.* **1993**, *30*, 583.

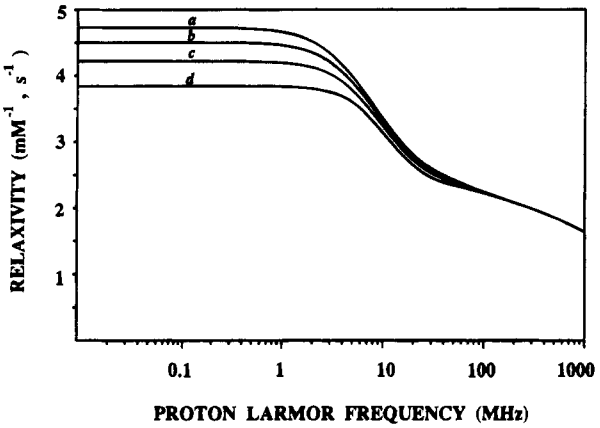

Figure 6. Simulated outer sphere NMRD profiles for values of the electronic relaxation time at zero field τ_{SO} of 120 (a), 100 (b), 80 (c), and 60 ps (d). Values typical of Gd(III) complexes were utilized for the other parameters: $\tau_V = 15$ ps, $a = 3.6$ Å, $D = 2.0 \times 10^{-5}$ cm^2 s^{-1}.

Table 1. Table of Best Fitting Parameters for Outer-Sphere Relaxivity

complex	T/°C	τ_{SO}/ps	τ_V/ps	a/Å	$D/10^5$ cm^2 s^{-1}
[Gd(**1**)]$^-$	5	70.8	23.6	4.25	1.1
[Gd(**1**)]$^-$	25	71.0	11.5	4.25	2.0
[Gd(**1**)]$^-$	35	85.1	10.7	4.25	2.8
[Gd(**2**)]$^-$	23	98.4	12.6	3.82	1.9
[Gd(**2**)]$^-$	37	94.8	7.44	3.82	2.8

range, even if with more pronounced effects at the low Larmor frequencies. The variation of D (Figure 5) changes the inflection point that moves toward higher fields with increasing D and has a large influence on the value of relaxitivity: a maximum in the low and high field regions and minimum in the intermediate region (~7−20 MHz). The effects of τ_{SO} variations on the profiles are reported in Figure 6: the high field region is not influenced by this parameter, but τ_{SO} is responsible for the large relaxivity changes in the low magnetic fields range. The variation of τ_V only causes minor changes in the profile in the region 1−100 MHz. On the basis of these observations we may qualitatively interpret the differences in the experimental profiles for [Gd(**1**)]$^-$ and [Gd(**2**)]$^-$ in Figure 3 as due to a sizable different value of a and small differences in the electronic relaxation time.

These considerations are fully confirmed by a best fitting procedure of the data with eqs 5 and 6 that yields the results reported in Table 1. As expected, the different relaxivity for [Gd(**1**)]$^-$ and [Gd(**2**)]$^-$ is accounted for by a difference of 0.43 Å in their a values, mainly attributable to their different size, with the complex of **1**, with its bulky benzylic groups, being less effective in relaxing the water protons. A further check of the validity of the above results is represented by the analysis of the NMRD profiles measured at different temperatures. In fact a correct best fitting analysis of the data taken at different temperatures should yield not only reasonable values for the parameters but also reproduce their expected temperature dependence.[11b] D should decrease with the increase of viscosity by lowering the temperature, a must be insensitive to temperature changes, τ_{SO} should vary very little, and τ_V should increase by decreasing the temperature. In Figure 7 are reported the NMRD profiles of [Gd(**1**)]$^-$ at 5 and 35 °C and of [Gd(**2**)]$^-$ at 37 °C. The "best fitting" results, in Table 1, confirm the above hypotheses and further validate the analysis at 25 °C.

Interaction of [Gd(1)]$^-$ with Bovine Serum Albumin (BSA). Preliminary MRI results showed a remarkably high

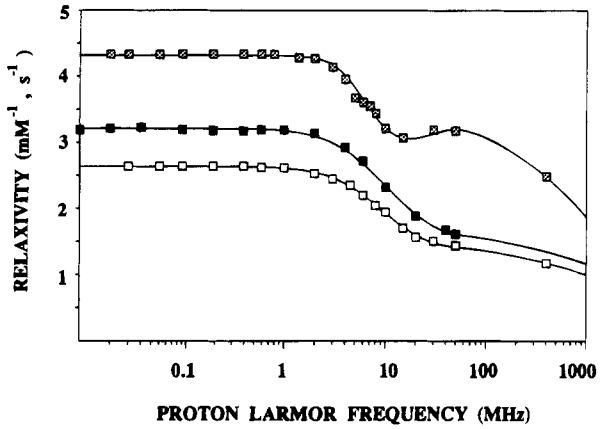

Figure 7. Experimental NMRD profiles for [Gd(**1**)]$^-$ at 5 °C (⊡) and 35 °C (□) and for [Gd(**2**)]$^-$ at 37 °C (■). The solid lines through the data have been calculated with the parameters of table 1.

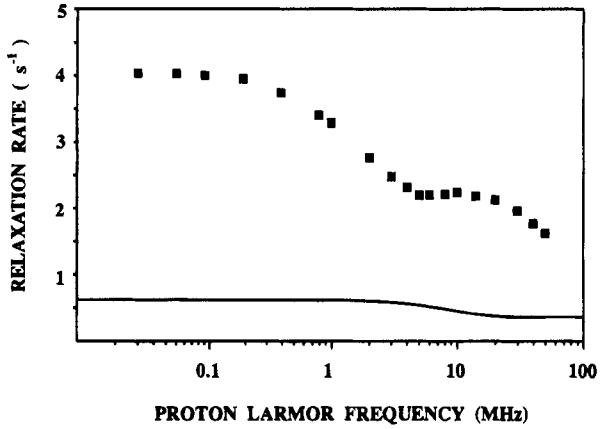

Figure 8. Experimental NMRD profile (298K) for [Gd(**1**)]$^-$ (0.2 mM) in the presence of bovine serum albumin (1.8 mM). The solid line at the bottom is the calculated profile for the same concentration of the complex in the absence of protein.

enhancing capability of [Gd(**1**)]$^-$ in liver and bile.[7,20] Actually the biliary excretion has to be expected for such an anionic complex bearing four hydrophobic benzylic groups. Although an understanding of the precise reason for the excretion pathway is very difficult, it is worthwhile to investigate, in some detail, the interaction of [Gd(**1**)] with a representative protein, serum albumin.

The $1/T_1$ NMRD profile of a 0.2 mM solution of [Gd(**1**)]$^-$ in the presence of 1.8 mM bovine serum albumin (BSA) is reported in Figure 8. The increase in solvent proton relaxation rate is impressive and suggests for this complex potential application as a hepatobiliary contrast agent. High relaxation enhancements upon interaction with albumin for complexes with hydration number $q = 0$ have been reported in the case of [Fe(5-Br-EHPG)]$^-$ and [Fe(5-Br-HBED)]$^-$.[23] In fact, although there is a certain variation in τ_D following the tight noncovalent binding to the macromolecule, this only accounts partially for the observed relaxation enhancement. It is plausible that a major contribution arises from the exchange of mobile protons on the protein which are "dipolarly relaxed" by the proximity to the paramagnetic ion.[21] Furthermore, the well-known occurrence of spin diffusion in the proton sink of the macromolecule provides an amplification of the induced effect. The large effects observed in this case suggest that a relaxivity gain for

(20) Rowland, I.; Leach, M. O.; Parker, D. *Abstracts of the 10th Congress of the European Society for Magnetic Resonance in Medicine and Biology*; 1993; p 432. Unpublished observations.
(21) Coolbaugh, L. C.; Bryant, R. B. *Magn. Reson. Med.* **1992**, *24*, 236.

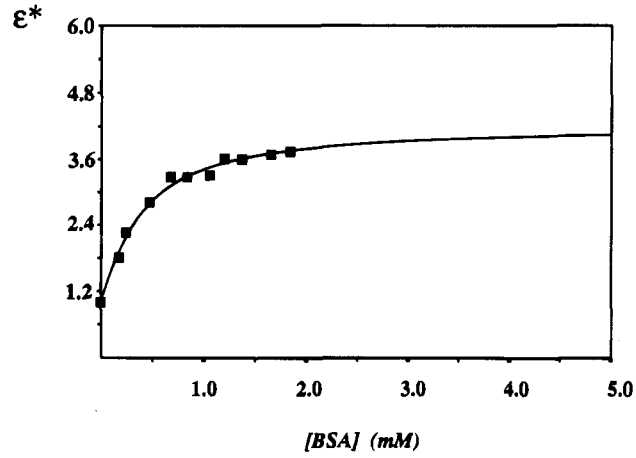

Figure 9. Proton relaxation enhancement for $[Gd(\mathbf{1})]^-$ (0.2 mM), at 20 MHz and 25 °C, as a function of bovine serum albumin concentration. The solid curve represents the best fit to eq 6 with the value of the parameters given in the text.

MRI applications may also be obtained by exploiting the proton exchange of a diamagnetic system dipolarly relaxed by a tight interaction with a paramagnetic center.

The strength of the interaction has been evaluated by calculating the dissociation constant K_d for the $[Gd(\mathbf{1})]$–BSA adduct through the proton relaxation enhancement technique.[22] The method involves monitoring, at a fixed proton Larmor frequency, the increase in relaxivity detectable when a certain concentration of the Gd complex is titrated with an increasing amount of the interacting biomolecule. By defining ϵ^*, the relaxivity enhancement factor, as the ratio of the paramagnetic relaxation rates in the presence and absence of macromolecule and ϵ_b as the limiting value for infinite concentration of macromolecule (i.e. the relaxivity enhancement of the bound complex), we can report the titration data as a plot of ϵ^* as a function of BSA concentration (Figure 9). In this form the experimental data can be analysed according to

$$\epsilon^* = (\epsilon_b^{-1}) \times \frac{C_T + nM_T + K_D - [(C_T + nM_T + K_D)^2 - 4nM_TC_T]^{1/2}}{2C_T} + 1$$

where C_T is the total concentration of the complex, M_T is the total concentration of BSA, and n is the number of independent and equivalent binding sites on the protein. From a best fitting procedure of data to the above equation, assuming that $n = 1$, we obtained a K_d value of 2.8×10^{-4}, indicative of a strong interaction and only about 1 order of magnitude larger than the value found for the tight binding site of a magnanese(II) ion.[24] The preference for only one binding site represents an assumption since the best fitting of the results is rather insensitive to the value of n. Furthermore, this kind of experiment can only highlight and yield information about the tight binding sites, and thus the presence of a number of low affinity binding sites on the protein cannot be excluded. Finally it is worth noting that the high value obtained for the limiting value of ϵ^* is a further and a clear indication of the large relaxivity gain that is attainable for an "outer-sphere" paramagnetic complex following the interaction with a slowly tumbling system.

An experiment was also performed to assess the hydration state of the complex when bound to the protein. The complex $[Tb(\mathbf{1})]^-$ (10^{-4} mol dm^{-3}) in H_2O (phosphate buffered saline at pH 7.4), in the presence of BSA (10^{-3} mol dm^{-3}) was examined by monitoring the decay of the characteristic Tb^{3+} luminescence emission at 545nm, following pulsed excitation. Under these conditions, and with a K_d value of 2.8×10^{-4}, the concentration of protein bound complex will be approximately 3 times that of the unbound complex. Thus the measured luminescence lifetime will be an average for that of the bound and unbound complex weighted towards that of the protein-bound complex. Experiments were carried out in both H_2O and D_2O, and the lifetimes were found to be 3.7(0.2) and 3.9(0.3) ms respectively. Although these values are very slightly lower than those found in the absence of the protein, they suggest a hydration state of 0.06 (the q value in Horrocks' method[32]) which compares to a value of 0.07 for the unbound complex. Clearly the hydration state of the complex is unperturbed by protein binding.

X-ray Crystal Structures of Ligand 1 and Its Yttrium Complex. Crystal Structure of $[(\mathbf{1})H]^+Cl^-$. In the crystal structure of the monohydrochloride salt of **1**, the asymmetric unit comprises one macrocyclic cation, one Cl^-, anion and six crystallization water molecules, of which two appear to be disordered. In the cation (Figure 10a), the tetraazacyclododecane ring has a "square" {3333} conformation,[33] in which all four nitrogen atoms are coplanar and point to one side of the ring, and all methylene hydrogen atoms are staggered. This conformation, corresponding to that of lowest strain energy,[33] has been observed previously in noncoordinated tetraazacyclododecane compounds.[34,35] All side chains are aligned in a cis fashion, i.e. on one side of the tetraazacyclododecane ring, and four of their oxygen atoms are directed inward, namely O(11), O(21), O(31) and O(41); together with four nitrogen atoms whose lone pairs all accordingly are directed inward, thus providing a binding site which is predisposed for 8-fold coordination of a metal ion.

Two of the nitrogen atoms, N(1) and N(3), are protonated, as can be seen from the relevant N–C bond distances, which average 1.52 Å (vs 1.48 Å for N(2) and N(4)). These atoms form hydrogen bonds with the adjacent inward looking oxygens, the N(1)···O(11) and N(3)···O(31) distances being shorter than N(2)···O(21) and N(4)···O(41) (2.83 and 2.93 Å vs. 2.99 and 3.24 Å) and the corresponding N–C–P–O torsion angles smaller for the former two (22 and 5° vs 42 and 65°, respectively). Although H atoms were not located, the protonation of O(21) and O(41) is apparent from their P–O bond

(22) Aime, S.; Botta, M.; Panero, M.; Grandi, M.; Uggeri, F. *Magn. Reson. Chem.* **1991**, *29*, 923.
(23) Lauffer, R. B.; Brady, T. J. *Magn. Reson. Imaging* **1985**, *3*, 11. Jenkins, B. F.; Armstrong, F.; Lauffer, R. B. *Magn. Reson. Imaging* **1991**, *17*, 164.
(24) Mildvan, A. S.; Cohn, M. *Biochemistry* **1963**, *2*, 910.
(25) Murru, M.; Parker, D.; Williams, G.; Beeby, A. *J. Chem. Soc., Chem. Commun.* **1993**, 1116.
(26) Bryden, C. C.; Reilley, C. N. *Anal. Chem.* **1982**, *54*, 610.
(27) Metcalf, D. H.; Ghirardelli, R. G.; Palmer, R. A. *Inorg. Chem.* **1985**, *24*, 634; **1986**, *25*, 2175.
(28) Zolin, V. F.; Koreneva, L. G. *Zh. Strukt. Khim.* **1980**, *21*, 66.
(29) Albin, M.; Horrocks, W. De W. *Inorg. Chem.* **1985**, *24*, 895.
(30) Bunzli, J. C. G. In *Lanthanide Probes in Life, Chemical and Earth Sciences, Theory and Practice*; Bunzli, J. C. G., Choppin, G. R., Eds.; Elsevier: Amsterdam, 1989.
(31) Peacock, R. D. *Struct. Bonding (Berlin)* **1975**, *22*, 83. Mason, S. F. *Struct. Bonding (Berlin)* **1980**, *39*, 43.
(32) Horrocks, W. de W.; Sudnick, D. R. *Acc. Chem. Res.* **1981**, *14*, 384.
(33) Dale, J. *Isr. J. Chem.* **1980**, *20*, 3.
(34) Sakurai, T.; Kobayashi, K.; Tsuboyama, K.; Tsuboyanma, S. *Acta. Crystallogr., Sect. B* **1978**, *34*, 1144.
(35) Borgen, G.; Dale, J.; Daasvatn, K.; Krane, J. *Acta. Chem. Scand., Ser. B.* **1980**, *B34*, 249.

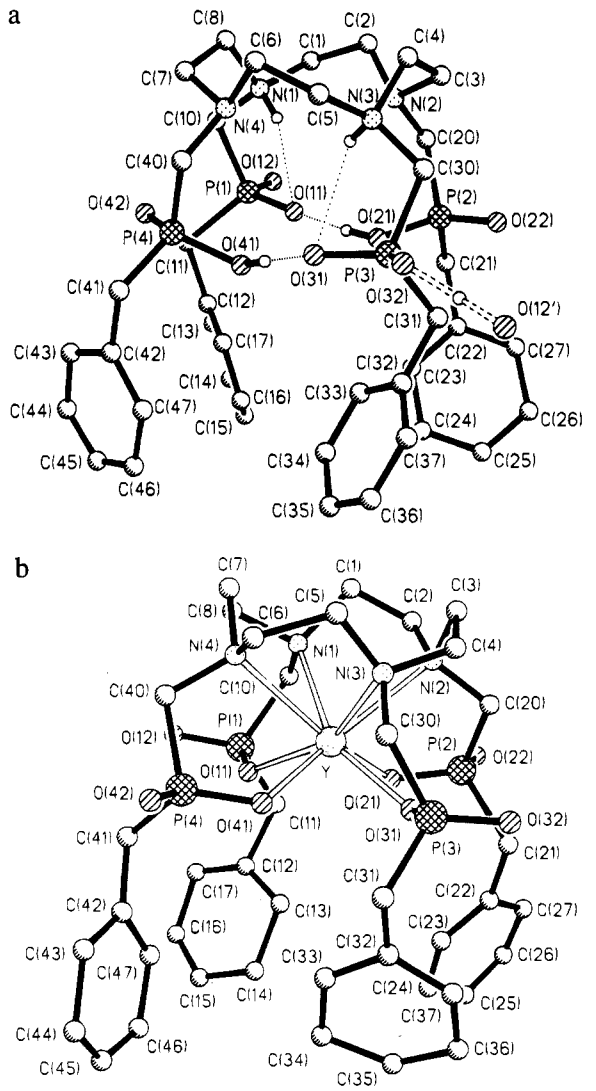

Figure 10. Molecular structures of (a) $[(\mathbf{1})H]^+Cl^-$, showing intra- and intercation hydrogen bonds, and (b) $[Y(\mathbf{1})]^-H_3O^+$, with phenyl and methylene hydrogens omitted.

distances, average 1.57 Å (characteristic of a single bond[36]). They form intramolecular hydrogen bonds O(21)H···O(11) and O(41)H···O(31) of 2.52 and 2.50 Å, the accepting oxygens of which already form double[36] P=O bonds (average 1.49 Å). Of the outward-looking oxygens, O(22) and O(42) form double P=O bonds (1.49 and 1.48 Å), while O(12) and O(32) participate in an intermolecular hydrogen bond and apparently have a proton situated between them, since their P—O bonds are of intermediate length (average 1.53 Å). A short O···O contact distance of 2.40 Å is typical for very strong hydrogen bonds, which are usually highly symmetrical.[37]

In the crystal, the cations of **1** are packed in layers, parallel to the (100) plane, with their pseudo-4-fold axis perpendicular to that plane. Molecules of the adjacent layers are antiparallel, so that interlayer contacts are of two types: benzyl-to-benzyl or macrocycle-to-macrocycle. In the latter case, the packing leaves wide channels, running parallel to the *z* axis, filled with Cl^- anions and water molecules, which are linked by hydrogen bonds into infinite chains, and at the same time to the outer O atoms of two neighboring layers (see Figure 11). The layers themselves can be subdivided into chains (also parallel to the *z* axis) linked by strong direct hydrogen bonds O12···O32. On the other hand, the "phenyl" sides of the layers are held together by van der Waals forces alone.

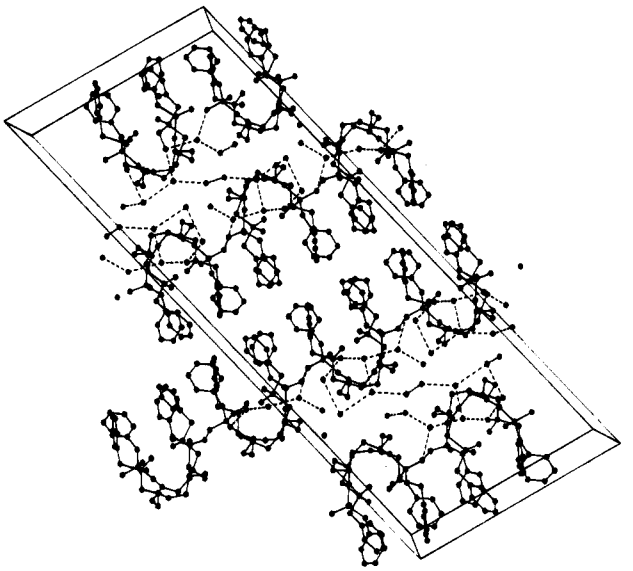

Figure 11. Crystal packing of $[(\mathbf{1})H]^+Cl^-$ (view down *y* axis) showing the hydrogen bonding system.

Hydrogen bond distances vary from 2.66 to 2.94 Å for water—water and water—phosphoxide bonds and 3.06 to 3.20 Å for water—chloride bonds. The O(5W)···O(6W) contact (2.39 Å) is probably spurious, as these positions seem to be only partially occupied.

Crystal Structure of $[Y.\mathbf{1}]^-H_3O^+$. In the structure of the yttrium complex $[Y(\mathbf{1})]^-$ (Figure 10b) the macrocyclic system retains approximately the same conformation as in the "free" ligand, i.e. in $[(\mathbf{1})H]^+Cl^-$ and the yttrium atom is coordinated to four (coplanar) nitrogen atoms and four phosphinate oxygens (also coplanar with each other). (A preliminary structural analysis of the Gd complex of **1** has revealed that it is isomorphous with $[Y(\mathbf{1})]^-$.) The yttrium atom is therefore not coordinated to a water molecule, as had been deduced from the NMRD profile of the related gadolinium complex and from the luminescence lifetimes of the related Tb(III) and Eu(III) complexes of **1** in H_2O and D_2O.[25] Indeed the nearest water molecule to Y is 5.62(2) Å distant (Y to O(2W)).

The coordination polyhedron of Y is a square prism twisted around the 4-fold axis. However, the angle of twist, $\psi = 29°$, lies well short of that for an idealized antiprism (45°). The configuration at each stereogenic phosphorus center is the same and the (*RRRR*) and (*SSSS*) enantiomers occur in ratio 1:1 in the unit cell.

It is well-known that the most common polyhedra for eight-coordinate complexes are the dodecahedron and the square antiprism.[38] The latter can be converted into the former by folding both square faces along their diagonals,[5] the folding angle δ being the measure of conversion ($\delta = 0$ for an antiprism and 29.5° for a dodecahedron).[39] The lanthanide complexes of 1,4,7,10-tetraazacyclododecane-1,4,7,10-tetraacetate (DOTA), $Na[Ln(DOTA)H_2O]\cdot 4H_2O$ are the closest analogues of $[Y(\mathbf{1})]^-$ studied to date. In isomorphous crystals with Ln = Eu, Gd,[9] and Y[10] the coordination polyhedron is an "undertwisted" ($\psi \approx 40°$) square antiprism, capped by one aqua ligand above the O_4 face. In a terbium(III) complex with 1,4,8,11-tetraazacyclotetradecane-1,4,8,11-tetraacetic acid (TETA),[5] where the terbium is eight-coordinated, the dodecahedral coordination is

(36) Allen, F. H.; Kennard, O.; Watson, D. G.; Brammer, L.; Orpen, A. G.; Taylor, R. *J. Chem. Soc., Perkin Trans. 2* **1987**, *Supplement*; 1.
(37) Elmsley, J. *Chem. Soc. Rev.* **1980**, *9*, 91.
(38) Drew, M. G. B. *Coord. Chem. Rev.* **1977**, *24*, 179.
(39) Porai-Koshits, M. A.; Aslanov, L. A. *J. Struct. Chem.* **1972**, *13*, 244.

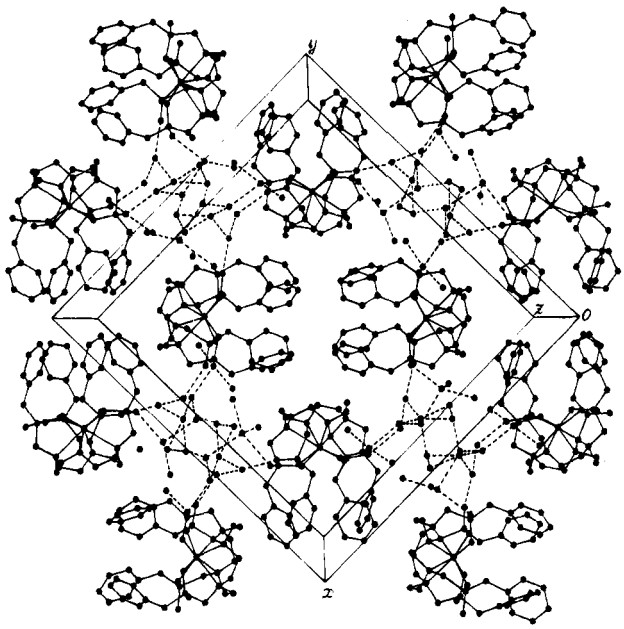

Figure 12. Crystal packing of $[Y(\mathbf{1})]^-$ (view down z axis) showing the hydrogen bonds.

severely distorted, and not toward the antiprism. It is noteworthy that the (empty) N_4O_4 polyhedron of $[(\mathbf{1})H]^+$ is strongly distorted (e.g. the O_4 face is folded by $\delta = 34°$, with the N_4 face remaining planar) and the introduction of the Y atom regularizes it, while at the same time generally contracting its size. It is instructive to compare the distances between the vertices of the N_4O_4 core and its center. In the free ligand these distances vary from 2.11 to 2.95 Å, with an average of 2.53 Å. In the yttrium complex these distances vary from 2.36 to 2.48 Å (average 2.44 Å). This observation is consistent with the relative flexibility of the present cyclopendant system, and suggests that the size of the intramolecular cavity may in fact be able to accommodate all lanthanide(III) ions, their ionic radii ranging from 1.01 (Ce) to 0.86 (Lu), as well as Y (0.90 Å).[40] However, the Y atom in $[Y(\mathbf{1})]^-$ does not occupy the center of the polyhedron, but is shifted by 0.33 Å toward the O_4 face. The Y–O distances are hence much shorter than the Y–N (average 2.26 Å vs 2.66 Å). The same pattern is observed in DOTA and TETA complexes[5,9,10] and is obviously due to the difference between donor–acceptor Y←N and highly ionic Y–O bonds, rather than to any minor difference between the N and O atoms ionic or covalent radii.[41]

P–O bond distances in $[Y(\mathbf{1})]^-$, averaging 1.53 Å for metal-coordinated oxygen atoms and 1.51 Å for noncoordinated ones, do not reveal protonation of any of these atoms. The position of the proton (needed for charge balance) remains unknown. Probably, one of the numerous water molecules in the structure (see below) is protonated, as occurs in the complexes of a $9N_3$ tris(phenylphosphinate) analogue with the divalent ions of copper, cobalt, zinc, and nickel.[43]

The torsion angles in the macrocycles of both $[(\mathbf{1})H]^+$ and $[Y(\mathbf{1})]^-$ form three groups: those around C–C bonds (average 58° in $[(\mathbf{1})H]^+$, 60° in $[Y(\mathbf{1})]^-$) and two conformationally nonequivalent groups of C–N bonds, e.g. N(1)–C(1) vs C(2)–N(2). These two groups give the averages of −161 and 79° in $[(\mathbf{1})H]^+$ vs −163 and 78° in the yttrium complex. These values are essentially the same as those found in DOTA complexes[9,10] and noncoordinated tetraazadodecanes.[33,34,35]

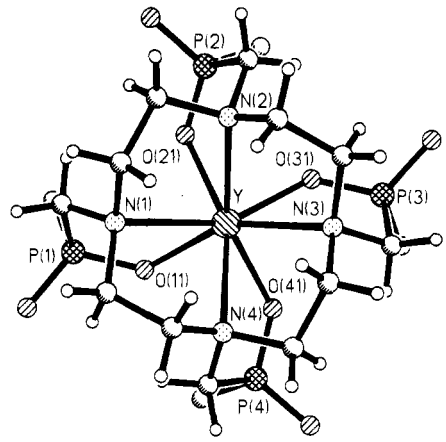

Figure 13. View down the C_4 axis in $[Y(\mathbf{1})]^-$ showing the layout of the phosphinate groups.

Crystal packing in the yttrium complex is completely different from that found in the monoprotonated ligand. The complex molecules, related via the 2_1 axis, form rows running parallel to the z axis, in which the pseudo-4-fold axis of neighbouring molecules are antiparallel and directed along the [1,1,0] or [1,−1,0] lines, i.e. almost perpendicular for different rows (see Figure 12). Between these rows, also parallel to z, run the channels occupied with water molecules, linking the host molecules into a three-dimensional framework by hydrogen bonds. Most of the water positions are disordered and/or are nonstoicheiometrically occupied. A few abnormally short O···O contacts (1.84–2.37 Å) prove that those positions cannot be occupied simultaneously.

Finally, it is worth emphasising that the suggestion made from an analysis of the NMR spectra of the Eu and Yb complexes of **1**, that the coordination polyhedron in $[Y(\mathbf{1})]^-$ would be quite distorted from a perfect antiprismatic geometry, is vindicated by the X-ray structural study. Indeed, the layout of the phosphinate groups in $[Y(\mathbf{1})]^-$ (Figure 13) is the same as that suggested for the minor isomer of $[YbDOTA]^-$ which was deduced from an analysis of the dipolar shifts in solution.[8]

Conclusions

The results may be summarized as follows.

(a) The yttrium complex of the tetrakis(benzylphosphinate) complex is eight-coordinate, is C_4 symmetric, and exists as a single diastereoisomer with no bound water molecule, as had been deduced in solution from luminescence measurements of the Eu and Tb complexes and from the analysis of the NMRD profile of the Gd complex.

(b) The crystal structures of the monoprotonated ligand and of the Y complex are very similar, suggesting that the ligand is favorably predisposed to bind lanthanide ions.

(c) The high resolution ^1H NMR spectra of Y–, Eu–, and Yb–**1** complexes reveal an unusual stereochemical rigidity of the ligand coordination cage.

(d) The $[Gd(\mathbf{1})]^-$ complex forms a strong 1:1 adduct with serum albumin leading to a very significant proton relaxation enhancement that correlates well with the strong and persistent signal enhancement observed with $[Gd(\mathbf{1})]^-$ in the selective imaging (MRI) of the bile duct/GT tract and in particular of tumor tissue, where slower clearance of $[Gd(\mathbf{1})]^-$ was observed (up to at least 8 h) compared to surrounding tissue, allowing tumors to be pinpointed clearly.[20]

(40) Shannon, R. D. *Acta Crystallogr., Sect. A.* **1976**, *32*, 751.
(41) Pauling, L. *The Nature of the Chemical Bond*, 3rd ed.; Cornell University Press: Ithaca, NY, 1960.
(42) Sheldrick, G. M. SHELXTLPLUS. Gottingen and Siemens, 1990.
(43) Cole, E.; Parker, D.; Ferguson, G.; Gallagher, J. F.; Kaitner, B. *J. Chem. Soc., Chem. Commun.* **1991**, 1473. Cole, E.; Parker, D.; Copley, R.; Howard, J. A. K.; Ferguson, G.; Gallagher, J. F. *J. Chem. Soc., Dalton Trans.* **1994**, 1619.

Table 2. Crystal Data and X-ray Experimental Details for $[(1)H]^+Cl^-$ and $[Y(1)]^-H_3O^+$

	$[(1)H]^+Cl^-$	$[Y(1)]^-H_3O^+$
formula	$[C_{40}H_{57}N_4O_8P_4]Cl\cdot 5H_2O$	$H[C_{40}H_{52}N_4O_8P_4Y]\cdot xH_2O^a$
M	971.3	1052.3
cryst syst	monoclinic	orthorhombic
a/Å	48.21(3)	22.332(5)
b/Å	11.455(4)	23.052(9)
c/Å	18.474(11)	21.301(8)
β/deg	103.88(4)	90
V/Å	9905(9)	10965(7)
space group	$C2/c$ (No. 15)	$Pbcn$ (No. 60)
Z	8	8
D_x/g cm^{-3}	1.30	1.28
$F(000)$	4128	4412
μ(Mo Kα)/cm^{-1}	2.7	12.4
cryst size/mm	0.15 × 0.30 × 0.58	0.2 × 0.4 × 0.5
cell dimens refinement		
no. of reflcns	20	30
2θ range/deg	11.0−25.7	12.1−23.0
no. of independent data	3135	3470
2θ max/deg	45	35
no. of obsd data, $\|F\| > 4\sigma(F)$	2484	1625
semiempirical abs cor		
no. of ψ-scans	360	390
no. of reflcns	10	13
transm coeff		
min	0.722	0.260
max	0.883	0.292
no. of variables	318	260
R	0.078	0.089
$R_w = R'$	0.103	0.099
goodness-of-fit	3.53	2.70
max. (Δ/σ)	0.01	0.18
residual $\Delta\rho$/eÅ^{-3}		
max	0.85	0.54
min	−0.38	−0.34

[a] $x = 6.75$ was used in calculations.

Experimental Section

The $1/T_1$ NMRD profiles were recorded from 2.5×10^{-4} to 1.4 T (0.01−50 MHz proton Larmor frequencies) on the Koenig−Brown relaxometers installed at the Department of Chemistry, University of Florence, Italy, for $[Gd(1)]^-$ and at the NMR Laboratory, University of Mons-Hainaut, Belgium, for $[Gd(2)]^-$. The relaxivity data at 90 and 400 MHz, included in some of the NMRD profiles, and the ^1H and ^{13}C high resolution NMR spectra were recorded on Jeol EX-90 and EX-400 spectrometers respectively. Proton relaxation rate titration data (20 MHz, 298 K) were measured on a Stelar Spinmaster (Pavia, Italy) spectrometer by means of the inversion recovery technique (16 experiments, four scans). The reproducibility in the relaxation rate measurements was ±0.5%. The temperature was controlled by a Jeol air flow heater, equipped with a copper−constantan thermocouple; the actual temperature in the probehead was measured with a Fluke 52k/j digital thermometer, with an uncertainty of 0.3 K. An 0.2 mM aqueous solution of the gadolinium complex was prepared by dilution from a 5 mM stock solution and the pH corrected to 6.8 with diluted HCl and NaOH. Weighed amounts of bovine serum albumin (fraction V, Merck), corresponding to a concentration range of 0.15−1.8 mM were then added to the solution under magnetic stirring. During the experiment, the pH of the solution did not change noticeably (±0.2 K).

Luminescence spectra were obtained using a Perkin-Elmer LS-50B instrument. The quoted lifetimes are the average of 10 separate measurements each of which is obtained by monitoring the phosphorescence intensity after 20 different time delays. Four excitation wavelengths were used (250, 305, 355, and 375 nm) with an excitation slit width of 10 nm. The emission slit width was 15 nm, and a gate time of 0.4 ms was used in each case. Solutions of the europium and terbium complexes were examined at a concentration of 1×10^{-4} mol dm^{-3} in the presence of bovine serum albumin (10^{-3} mol dm^{-3} in phosphate-buffered saline at pH 7.4 and 293 K). Bovine serum albumin was obtained from Sigma (A2153) and was used as received. The Eu, Tb, and Yb complexes were prepared and purified as described for the yttrium and gadolinium complexes, reported earlier.[3]

H_3O^+[Eu(1)]. To a solution of ligand **1** (0.25 g, 0.30 mmol) in Purite water (20 cm^3, giving a solution pH of 2), was added europium

Table 3. Atomic Coordinates ($\times 10^4$) and Equivalent Isotropic Displacement Coefficients (Å^2 × 10^3) in $[(1)H]^+Cl^-$

	x	y	z	U(eq)[a]
P(1)	3663(1)	1792(3)	2828(2)	44(2)
P(2)	3629(1)	5780(3)	3235(2)	45(2)
P(3)	3581(1)	5763(3)	5682(2)	46(2)
P(4)	3661(1)	1644(3)	5215(2)	47(2)
O(11)	3695(2)	2925(7)	3227(4)	48(3)
O(12)	3671(2)	1885(7)	2000(4)	56(4)
O(21)	3706(2)	4855(7)	3884(4)	49(3)
O(22)	3590(2)	6956(6)	3542(4)	53(4)
O(31)	3625(2)	4474(7)	5692(4)	54(4)
O(32)	3534(2)	6276(6)	6398(4)	52(4)
O(41)	3795(2)	2815(7)	5028(4)	54(4)
O(42)	3650(2)	763(7)	4624(4)	53(3)
N(1)	3122(2)	2189(8)	3033(5)	40(3)
N(2)	3102(2)	4775(8)	2982(5)	39(3)
N(3)	3092(2)	5020(7)	4601(5)	40(3)
N(4)	3111(2)	2420(8)	4669(5)	43(3)
C(1)	3007(2)	2860(10)	2318(6)	44(3)
C(2)	2888(2)	4044(10)	2473(6)	47(3)
C(3)	2956(2)	5745(10)	3279(6)	45(3)
C(4)	2848(2)	5373(10)	3945(6)	46(3)
C(5)	2970(2)	4322(10)	5151(6)	49(4)
C(6)	2879(2)	3079(10)	4863(6)	50(4)
C(7)	2997(2)	1404(10)	4193(6)	49(4)
C(8)	2886(2)	1734(10)	3364(6)	48(3)
C(10)	3313(2)	1216(9)	2886(6)	43(3)
C(11)	3923(2)	706(10)	3235(7)	54(4)
C(12)	4222(2)	1168(10)	3371(7)	50(4)
C(13)	4392(3)	972(12)	2884(7)	73(4)
C(14)	4674(3)	1403(13)	3033(9)	91(5)
C(15)	4774(3)	2035(14)	3650(9)	98(5)
C(16)	4617(3)	2228(14)	4129(9)	101(5)
C(17)	4338(3)	1822(12)	3992(8)	76(4)
C(20)	3311(2)	5251(10)	2598(6)	43(3)
C(21)	3907(2)	5757(11)	2741(6)	54(4)
C(22)	4181(3)	6176(11)	3194(7)	56(4)
C(23)	4385(3)	5426(14)	3570(8)	85(5)
C(24)	4644(3)	5819(16)	4024(9)	112(6)
C(25)	4691(4)	7028(16)	4120(9)	114(6)
C(26)	4492(4)	7790(17)	3767(9)	115(6)
C(27)	4234(3)	7353(14)	3294(8)	85(5)
C(30)	3257(2)	6076(10)	4976(6)	48(4)
C(31)	3867(2)	6542(10)	5438(6)	48(4)
C(32)	4148(2)	6084(10)	5827(6)	43(3)
C(33)	4270(3)	5212(12)	5513(8)	78(5)
C(34)	4532(3)	4749(14)	5883(9)	100(5)
C(35)	4671(3)	5143(14)	6578(9)	95(5)
C(36)	4546(3)	5987(13)	6889(8)	89(5)
C(37)	4291(3)	6446(12)	6527(7)	69(4)
C(40)	3312(2)	1976(11)	5356(6)	50(4)
C(41)	3865(2)	1156(11)	6091(7)	63(4)
C(42)	4169(3)	934(12)	6096(7)	59(4)
C(43)	4246(3)	−76(14)	5802(8)	94(5)
C(44)	4541(4)	−258(17)	5784(10)	121(6)
C(45)	4732(4)	493(17)	6087(9)	116(6)
C(46)	4671(4)	1431(17)	6398(10)	132(7)
C(47)	4378(3)	1678(14)	6411(8)	93(5)
Cl	2222(1)	3236(5)	3214(2)	115(2)
O(1W)	3446(2)	8583(7)	2318(5)	76(3)
O(2W)	2839(2)	8650(8)	3530(5)	93(3)
O(3W)	2512(3)	8567(11)	4597(7)	139(4)
O(4W)	3410(2)	8669(7)	4316(4)	69(3)
O(5W)	2162(4)	5583(17)	3949(10)	90(6)
O(6W)	3264(4)	1111(17)	680(10)	92(6)

[a] Equivalent isotropic U defined as one-third of the trace of the orthogonalized U_{ij} tensor.

Table 4. Atomic Coordinates ($\times 10^4$) and Equivalent Isotropic Displacement Coefficients ($Å^2 \times 10^3$) in $[Y(1)]^-H_3O^+$

	x	y	z	U(eq)[a]
Y	2294(1)	2342(1)	433(1)	63(1)
P(1)	1106(4)	2872(4)	1255(4)	72(4)
P(2)	1498(4)	2512(4)	−915(4)	74(4)
P(3)	3051(4)	1308(4)	−361(4)	80(4)
P(4)	2701(5)	1645(4)	1771(4)	76(4)
O(11)	1573(8)	2380(8)	1173(8)	67(6)
O(12)	995(9)	3060(9)	1927(10)	91(7)
O(21)	1471(8)	2410(8)	−222(8)	67(6)
O(22)	1021(9)	2913(8)	−1161(9)	90(7)
O(31)	2473(7)	1659(7)	−263(7)	57(6)
O(32)	3257(9)	1192(9)	−1039(10)	98(7)
O(41)	2560(7)	1610(7)	1077(8)	62(6)
O(42)	3215(9)	1301(9)	1998(8)	83(7)
N(1)	2063(11)	3436(10)	756(12)	88(9)
N(2)	2508(10)	3063(10)	−503(11)	76(8)
N(3)	3444(10)	2351(10)	89(11)	75(7)
N(4)	3025(10)	2715(11)	1340(10)	71(7)
C(1)	2284(15)	3840(13)	221(13)	108(12)
C(2)	2191(13)	3630(12)	−424(14)	91(10)
C(3)	3132(13)	3178(13)	−624(14)	92(12)
C(4)	3496(13)	2652(13)	−531(14)	98(11)
C(5)	3840(12)	2662(13)	549(12)	86(10)
C(6)	3645(12)	2528(12)	1213(13)	83(11)
C(7)	3023(13)	3341(13)	1409(14)	98(12)
C(8)	2396(14)	3569(13)	1350(13)	90(11)
C(10)	1392(11)	3471(12)	809(12)	77(10)
C(11)	408(13)	2702(14)	891(14)	115(12)
C(12)	144(9)	2145(8)	1104(11)	86(11)
C(13)	256	1614	813	133(15)
C(14)	1	1108	1050	132(14)
C(15)	−367	1132	1579	113(13)
C(16)	−479	1663	1870	116(13)
C(17)	−224	2169	1632	92(11)
C(20)	2242(13)	2798(12)	−1076(13)	88(10)
C(21)	1462(12)	1847(11)	−1336(13)	79(10)
C(22)	858(8)	1532(9)	−1280(12)	86(11)
C(23)	790	1141	−785	118(13)
C(24)	247	853	−700	162(17)
C(25)	−229	956	−1109	128(14)
C(26)	−161	1347	−1604	134(15)
C(27)	382	1635	−1690	114(13)
C(30)	3632(11)	1718(12)	60(13)	77(10)
C(31)	2981(11)	623(12)	44(13)	82(10)
C(32)	2406(7)	339(7)	−39(11)	76(10)
C(33)	2007	304	463	108(12)
C(34)	1458	23	388	108(12)
C(35)	1309	−222	−190	98(12)
C(36)	1708	−187	−692	105(12)
C(37)	2256	94	−617	94(11)
C(40)	2825(13)	2407(12)	1894(13)	92(11)
C(41)	2046(11)	1490(11)	2241(12)	71(10)
C(42)	1841(11)	865(7)	2273(9)	76(10)
C(43)	2173	430	2567	125(14)
C(44)	1935	−127	2627	154(16)
C(45)	1366	−249	2393	119(13)
C(46)	1034	185	2099	103(12)
C(47)	1271	742	2039	89(11)
O(1W)	5000	1506(16)	7500	162(15)
O(2W)	1836(13)	3020(14)	2922(14)	126(12)
O(3W)	3703(16)	1024(16)	3149(16)	188(16)
O(4W)	4892(16)	1521(16)	4325(16)	186(16)
O(5W)	4375(18)	1121(16)	1617(18)	108(16)
O(6W)	4411(18)	1031(16)	8724(18)	104(15)
O(7W)	3383(20)	95(20)	1601(20)	144(19)
O(8W)	4885(24)	491(20)	7916(21)	166(23)
O(9W)	5013(24)	759(22)	5250(23)	177(23)
O(10W)	3868(24)	747(24)	7283(23)	183(23)
O(11W)	4337(36)	45(34)	5604(37)	114(31)
O(12W)	4518(34)	2051(32)	2605(36)	97(29)
O(13W)	3390(36)	321(34)	8112(36)	106(30)
O(14W)	4111(40)	476(38)	4436(42)	142(37)

[a] Equivalent isotropic U defined as one-third of the trace of the orthogonalized U_{ij} tensor.

Table 5. Selected Bond Lengths (Å) and Bond Angles (deg) in $[(1)H]^+Cl^-$ and $[Y(1)]^-H_3O^+$ (Esd in Parentheses)

Bond Distances

$[(1)H]^+$

P(1)−O(11)	1.483(8)	P(2)−O(22)	1.490(8)
P(1)−O(12)	1.542(8)	P(2)−C(20)	1.802(10)
P(1)−C(10)	1.838(11)	P(2)−C(21)	1.791(13)
P(1)−C(11)	1.798(11)	N(1)−C(1)	1.514(13)
P(2)−O(21)	1.575(8)	N(1)−C(8)	1.508(15)

$[Y(1)]^-$

Y−O(11)	2.26(2)	Y−N(4)	2.67(2)
Y−O(31)	2.20(2)	P(1)−O(11)	1.55(2)
Y−N(1)	2.66(2)	P(1)−O(12)	1.52(2)
Y−N(3)	2.67(2)	P(1)−C(10)	1.79(3)
Y−O(21)	2.31(2)	P(1)−C(11)	1.79(3)
Y−O(41)	2.26(2)	P(2)−O(21)	1.50(2)
Y−N(2)	2.64(2)	P(2)−O(22)	1.50(2)

Bond Angles

$[(1)H]^+$

O(11)−P(1)−O(12)	114.1(5)	C(1)−N(1)−C(8)	111.9(8)
O(11)−P(1)−C(10)	106.0(5)	C(1)−N(1)−C(10)	109.3(8)
O(12)−P(1)−C(10)	109.0(5)	P(1)−C(10)−N(1)	110.6(7)
O(11)−P(1)−C(11)	114.7(5)	P(1)−C(11)−C(12)	111.8(8)
C(10)−P(1)−C(11)	106.5(5)		

$[Y(1)]^-$

O(11)−Y−O(21)	81.4(6)	N(1)−Y−N(3)	104.5(7)
O(11)−Y−O(31)	128.9(6)	N(2)−Y−N(3)	67.3(7)
O(21)−Y−O(31)	77.7(6)	O(21)−Y−N(3)	126.8(6)
O(11)−Y−O(41)	78.0(6)	O(31)−Y−N(3)	69.3(7)
O(21)−Y−O(41)	128.8(6)	O(11)−Y−N(4)	85.3(6)
O(31)−Y−O(41)	80.0(6)	O(21)−Y−N(4)	154.1(7)
N(1)−Y−N(2)	68.6(7)		

oxide (0.05 g, 0.15 mmol) and the mixture was heated to reflux for 18 h to give a white suspension. After the pH was adjusted to 6.5 (1% NaOH solution), the mixture was heated under reflux for a further 2 h, and after cooling it was filtered (0.45 μm filter) to yield a colorless solution. After concentration to small volume (ca. 4 cm^3), the solution was left to crystallize at 4 °C to yield a colorless crystalline solid (0.19 g, 60%). Anal. Calcd for $C_{40}H_{55}N_4O_9P_4Eu·6H_2O$: C, 43.6; H, 6.09; N, 5.08. Found: C, 43.4; H, 6.31; N, 5.29. δ_H (D_2O, pD 6): −17.99 (4H, CH*H*P); −11.41, (4H, C*H*HP); −7.51 (4H, C*H*HN ring); −4.50 (4H, CH*H*N ring); −2.08 (4H, PCH_2Ph); −0.72 (4H, CH_2Ph); 0.75 (4H, $N'CH_2$ ring); 9.47 (4H, para-H, Ar); 10.78 (8H, meta-H, Ar); 14.08 (8H, ortho-H, Ar); 34.40 (4H, $N'CH_2$) $\delta p[^1H]$ (D_2O) + 86.1 ppm. MS, *m/e* (FAB.; *m*-nitrobenzyl alcohol): 994 (100%, $M^+ + 1$).

H_3O^+[Tb(1)]. This was prepared as described above for the europium complex. Anal. Calcd for $C_{40}H_{55}N_4O_9P_4Tb·6H_2O$: C, 43.1; H, 6.02; N, 5.03. Found: C, 42.8; H, 6.39; N, 4.81. $\delta p[^1H]$ (D_2O): +547 ppm. MS, *m/e* (FAB): 1001, ($M^+ + 1$, 100%).

X-ray Diffraction Structural Study. Crystals of $[(1)H]^+Cl^-·5H_2O$ and $[Y(1)]^- H_3O^+·6.75H_2O$ were grown from water. X-ray diffraction experiments with **1** and [Y(1)] were carried out at room temperature using a MicroVAX-controlled Siemens R3m/V four-circle diffractometer, graphite-monochromated Mo Kα radiation (λ = 0.710 73 Å), and Wyckoff (limited ω) scan mode. The crystals were sealed in Lindemann glass capillaries with solvent (water).

Crystal data and experimental details are listed in Table 2. The structures were solved by direct (for $[(1)H]^+Cl^-$) and by Patterson (for $[Y(1)]^-H_3O^+$) methods and were refined by full-matrix least-squares methods using SHELXTLPLUS programs.[42] For **1**, the phosphorus, chlorine, and phosphorus-bound oxygen atoms were refined with anisotropic displacement factors and the rest of the non-hydrogen atoms isotropically. The C- and N-bound hydrogen atoms were treated in the riding model although the O-bound ones were not located. For the yttrium complex, Y and P atoms were refined with anisotropic displacement factors, phenyl groups in a rigid-body model, and the rest of the non-hydrogen atoms in an isotropic approximation (with riding H atoms for phenyl and CH_2 groups). Weighting schemes $w^{-1} = \sigma^2(F) + 0.0004F^2$ were used for both structures.

Within the asymmetric unit of $[(1)H]^+Cl^-·5H_2O$, six positions of solvate water molecules were revealed, of which O(1W) to O(4W) were

refined with 100% occupancy factors, and O(5W) and O(6W) with 50% factors, according to electron density peak maxima and the refinement of thermal factors of these atoms. For the yttrium complex, the difference Fourier map exhibited a highly diffuse distribution of electron density in intermolecular space, which was interpreted as 14 independent positions of crystallization water molecules. Of these, atoms O(1W) (on the 2-fold axis) and O(5W) to O(10W) were refined with occupancy factors of 50%, O(2W) to O(4W) with 75%, and O(11W) to O(14W) with 25%. These assignments are, however, rather arbitrary, given the lack of high-angle reflections available. The O(8W) and O(12W) atoms are unreasonably close to their symmetrical (via a 2-fold axis) equivalents (1.84 and 2.20 Å). This fact and the short contacts O(10W)···O(13W) = 2.29 and O(9W)···O(11W) = 2.36 Å also confirm the nonstoichiometric occupancy of these positions.

Final atomic coordinates are listed in Tables 3 and 4 with selected bond distances and angles in Table 5. Additional material is available from the Cambridge Crystallographic Data Centre and comprises H atom coordinates, thermal parameters, and the remaining bond distances and angles.

Acknowledgment. We thank for support the MRC (K.S.) and the Royal Society (A.S.B.).

Supplementary Material Available: Listing of hydrogen atom coordinates, thermal parameters and bond distances and angles for the X-ray structures of $[(\mathbf{1})H]^+Cl^-$ and $H_3O^+[(\mathbf{1})Y]^-$ (12 pages). Ordering information is given on any current masthead page.